Article

Methane formation driven by light and heat prior to the origin of life and beyond

Leonard Ernst [1,2] ✉, Uladzimir Barayeu [3,4], Jonas Hädeler [5], Tobias P. Dick[3,4], Judith M. Klatt[2,6,7], Frank Keppler [5,8] & Johannes G. Rebelein [1,2] ✉

Methane is a potent greenhouse gas, which likely enabled the evolution of life by keeping the early Earth warm. Here, we demonstrate routes towards abiotic methane and ethane formation under early-earth conditions from methylated sulfur and nitrogen compounds with prebiotic origin. These compounds are demethylated in Fenton reactions governed by ferrous iron and reactive oxygen species (ROS) produced by light and heat in aqueous environments. After the emergence of life, this phenomenon would have greatly intensified in the anoxic Archean by providing methylated sulfur and nitrogen substrates. This ROS-driven Fenton chemistry can occur delocalized from serpentinization across Earth's humid realm and thereby substantially differs from previously suggested methane formation routes that are spatially restricted. Here, we report that Fenton reactions driven by light and heat release methane and ethane and might have shaped the chemical evolution of the atmosphere prior to the origin of life and beyond.

Methane (CH_4) is a potent greenhouse gas which has in the past and is still today contributing to climate change[1]. Atmospherically accumulated CH_4 and ethane (C_2H_6) might also explain the "faint young sun paradox", which describes the apparent contradiction of a fainter sun (70 – 83% of the current solar energy output) but a climate that was at least as warm as today during early Earth (4.5–2.5 Ga ago)[2–4]. Although these CH_4 levels would be essential to keep the Earth a liquid hydrosphere to allow the evolution of life during the Archean (4.0–2.5 Ga), the source of CH_4 prior to the origin of life is still under debate[5]. While CH_4 was released by submarine volcanism, most CH_4 is suggested to be formed as side product of serpentinization[5]. After the evolution of microbial methanogenesis latest by 3.5 Ga[6], methanogenesis could have been responsible for a CH_4 flux comparable to today[7]. Thus, methanogenesis is expected to be the main source of CH_4 during the Archean, supported by light carbon isotope values in sedimentary deposits[8]. However, isotope signals can only manifest upon reoxidation and CH_4 itself does not leave much of a signature in the geological record. Thus, the actual CH_4 concentrations and the potential abiotic sources during early Earth remain elusive. Based on mass-independent fractionation of sulfur, at least 20 ppmv CH_4 was present around 2.4 Ga ago[9]. A more recent study analyzing the fractionation of xenon isotopes suggests CH_4 levels of >5000 ppmv around 3.5 Ga ago[10]. Catling et al. expect even higher CH_4 levels at the beginning of the Archean (4 Ga)[3] before methanogenesis evolved. Yet, the processes responsible for these high CH_4 levels and their relative contributions remain controversial.

Recently, we discovered a non-enzymatic CH_4 formation mechanism expected to occur in all living organisms[11]. The mechanism has been demonstrated to be active in over 30 very diverse organisms[11] and suggested to explain previously observed CH_4 formation by cyanobacteria[12], freshwater and marine algae[13,14], saprotrophic fungi[15] and plants[16]. The CH_4 formation is driven by a cascade of radical reactions, governed by the interplay of reactive oxygen species (ROS) and ferrous iron (Fe^{2+}), methylated sulfur (S)- and nitrogen (N)-compounds

[1]Max Planck Institute for Terrestrial Microbiology, 35043 Marburg, Germany. [2]Center for Synthetic Microbiology (SYNMIKRO), 35032 Marburg, Germany. [3]Division of Redox Regulation, German Cancer Research Center (DKFZ), DKFZ-ZMBH Alliance, 69120 Heidelberg, Germany. [4]Faculty of Biosciences, Heidelberg University, 69120 Heidelberg, Germany. [5]Institute of Earth Sciences, Heidelberg University, 69120 Heidelberg, Germany. [6]Microcosm Earth Center, Max Planck Institute for Terrestrial Microbiology & Philipps University Marburg, 35032 Marburg, Germany. [7]Biogeochemistry Group, Department for Chemistry, Philipps University Marburg, 35032 Marburg, Germany. [8]Heidelberg Center for the Environment HCE, Heidelberg University, 69120 Heidelberg, Germany. ✉e-mail: leonard.ernst@mpi-marburg.mpg.de; johannes.rebelein@mpi-marburg.mpg.de

are oxidatively demethylated by hydroxyl radicals (•OH) and oxo-iron(IV) complexes ($[Fe^{IV}=O]^{2+}$) to yield methyl radicals (•CH_3)[11].

Here we show that this abiotic mechanism occurs also outside living cells and might have contributed to CH_4 levels before life emerged. All needed components: (i) methylated S- and N-compounds, (ii) Fe^{2+} and (iii) ROS are found under early-earth conditions. (i) In a prebiotic world, methylated S-compounds like methanethiol, dimethyl sulfide (DMS) or dimethyl sulfoxide (DMSO) were formed abiotically under the reducing conditions of hydrothermal vents[17–19] or transported to Earth by carbonaceous meteorites during early Earth meteorite bombardment[20,21]. Upon the emergence of life, more methylated S-/N-compounds were produced by cells and organisms, i.e. methionine, dimethylsulfoniopropionate or trimethylamine[22]. (ii) Under the anoxic conditions of the early Earth, oceans were rather ferruginous, i.e. rich in Fe^{2+} required for Fenton chemistry[23,24], nonetheless ferric iron (Fe^{3+}) also occurred in Archean seawater[25]. Additionally, the mechanism driven by Fe^{2+} can be enhanced by Fenton-promoting Fe^{2+}-chelators, e.g. ATP or citrate[26]. Under anoxic conditions, Fe(III)-carboxylate complexes are photochemically reduced via ligand-to-metal charge transfer (LMCT)[27], resulting in Fe^{2+} and organic radicals[28]. (iii) Under ambient temperatures, low ROS levels exist in water that increase with heat[29], or can be generated by photolysis or radiolysis[30–33]. Under acidic

conditions, i.e. in volcanic lakes[34], illumination of Fe(III)-aqua complexes ($[Fe(H_2O)_6]^{3+}$) forms Fe^{2+} and ROS[35,36]. Thus, we hypothesized that the Fenton reaction of Fe^{2+} with H_2O_2, generated by heat and light, could have driven the formation of CH_4 from methylated S-/N-compounds independent of temperatures and pressures occurring at hydrothermal vents but at ambient conditions as early as the prebiotic world of the Hadean (4.5–4.0 Ga, Fig. 1a). To identify critical components of such a mechanism, we used aqueous model systems to determine the influence of heat, light, and (bio)molecules on CH_4 formation in abiotic and biotic environments.

Results

Methane is formed under abiotic conditions

To investigate CH_4 formation under abiotic conditions (Fig. 1a), we designed a chemical model system consisting of a nitrogen atmosphere, a potassium phosphate-buffered solution (pH 7, expected during the Archean at 4.0 Ga[37]) supplemented with Fe^{2+} and the abiotically formed DMSO which serves as methyl donor for ROS-driven CH_4 formation. Over the course of the experiments, no pH change was observed, while low amounts of $Fe(OH)_2$ precipitated. In this model system, CH_4 was consistently formed from DMSO in the dark (Fig. 1b). CH_4 formation rates increased with rising temperatures from 30 to 97 °C, consistent
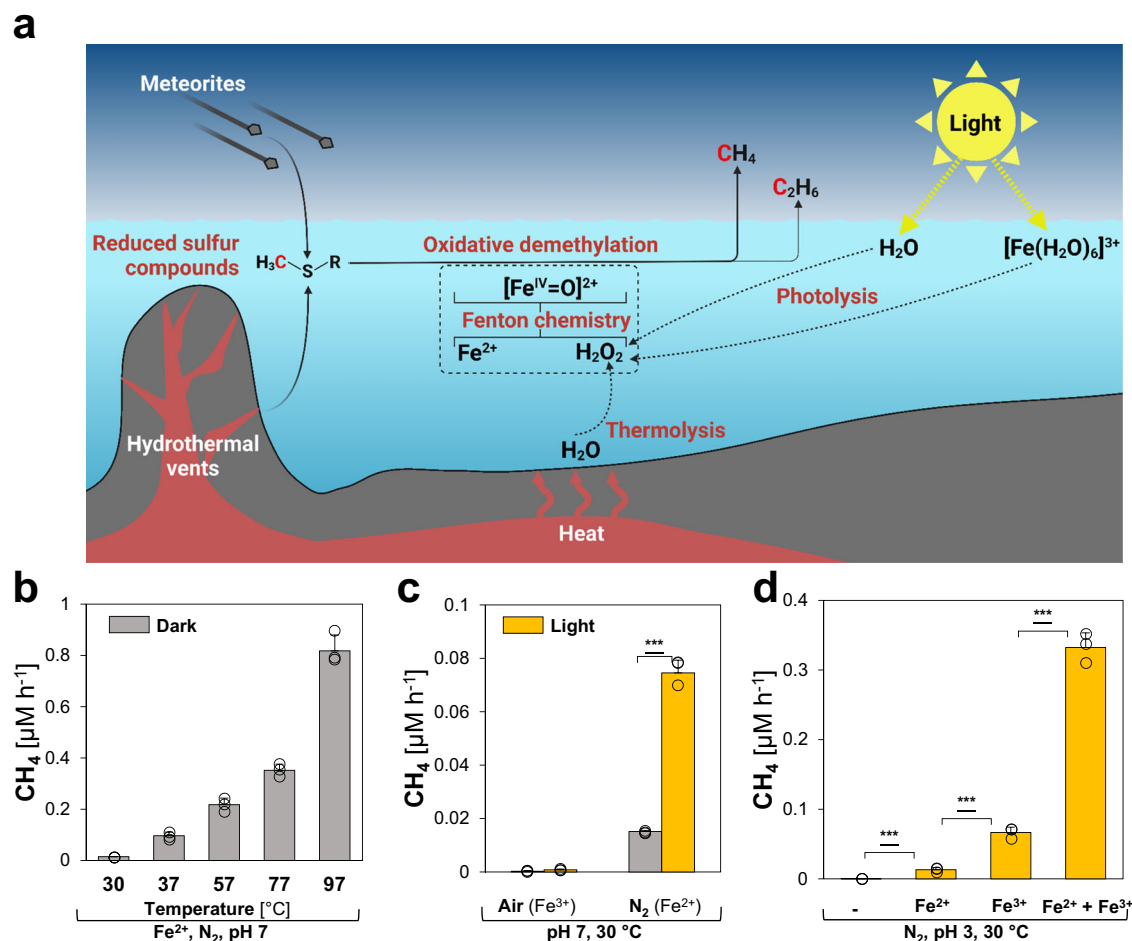

Fig. 1 | Heat and light drive CH₄ formation under abiotic conditions. a Reduced, methylated S-/N-compounds are formed abiotically in hydrothermal vents or transported to Earth by carbonaceous meteorites. Under anoxic conditions, H_2O_2 is formed by thermolysis and photolysis of water and $[Fe(H_2O)_6]^{3+}$ complexes, reacting with dissolved ferrous iron (Fe^{2+}) to hydroxyl radicals (•OH) and $[Fe^{IV}=O]^{2+}$ compounds that drive the oxidative demethylation of methylated S-/N-compounds, thereby facilitating CH_4 and C_2H_6 formation. **b** Thermolysis: CH_4 is formed from DMSO under high temperatures. **c** Water photolysis: The formation of CH_4 is

increased by light. **d** $[Fe(H_2O)_6]^{3+}$ photolysis: Under acidic conditions, light-driven CH_4 formation is enhanced by $[Fe(H_2O)_6]^{3+}$ photochemistry. All experiments were conducted in closed glass vials containing buffered solutions (pH 7 or pH 3) supplemented with DMSO and Fe^{2+} or Fe^{3+} at 30 °C (**b**, **c**) under a N_2 or air atmosphere. Statistical analysis was performed using paired two-tailed t tests, ***$p \leq 0.001$. The bars are the mean + standard deviation of triplicates, shown as circles. **a** Was created with BioRender.com.
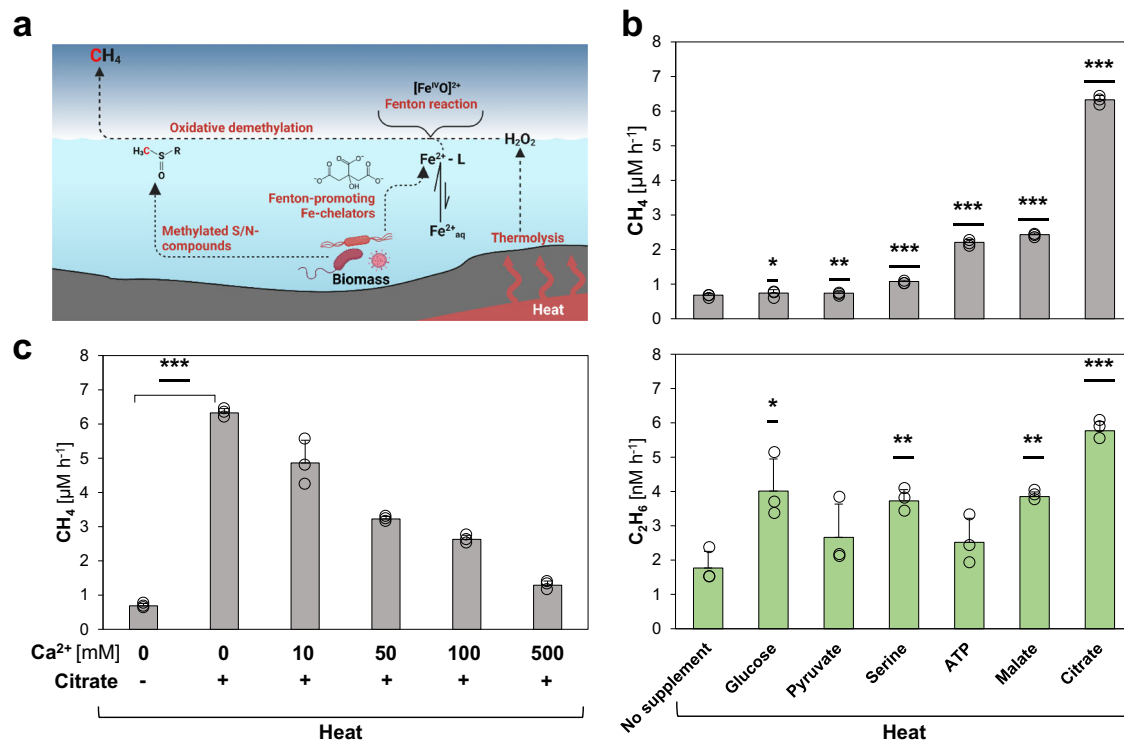
Fig. 2 | (Bio)molecules enhance heat-driven CH$_4$ formation. a Overview of CH$_4$ formation driven by heat. Living organisms produce S-/N-methylated compounds that serve as substrates for CH$_4$ formation and Fe^{2+}-chelators that promote Fenton chemistry and enhance CH$_4$ formation. **b** Heat-driven CH$_4$ (upper panel) and C$_2$H$_6$ (lower panel) formation is enhanced upon supplementation with (bio)molecules. **c** Citrate enhances heat-driven CH$_4$ formation acting as iron-chelator. Upon the addition of Ca^{2+}, CH$_4$ levels decrease due to the replacement of Fenton-promoting Fe^{2+}-citrate complexes with Ca^{2+}-citrate complexes. All experiments were conducted in closed glass vials containing a buffered solution (pH 7) supplemented with DMSO, Fe^{2+} and, optionally, citrate and Ca^{2+} under a pure nitrogen atmosphere at 97 °C (heat). Statistical analysis was performed using paired two-tailed *t* tests, *$p \le 0.05$, **$p \le 0.01$, ***$p \le 0.001$. The bars are the mean + standard deviation of triplicates, shown as circles. **a** Was created with BioRender.com.

with the previously reported temperature-dependency of ROS levels in water[29]. While only marginal CH$_4$ formation rates derived from DMSO were observed at 30 °C (~0.02 μM h^{-1}), rates increased 41-fold to ~0.82 μM h^{-1} at 97 °C. In addition, low C$_2$H$_6$ amounts were formed (Supplementary Fig. 1), most likely resulting from the recombination of two methyl radicals[23]. At 37 °C, the CH$_4$:C$_2$H$_6$ ratio was ~110, with an increasing trend towards higher temperatures. As the ROS-driven CH$_4$:C$_2$H$_6$ ratios are substantially lower than those observed for archaeal methanogenesis[38], the CH$_4$:C$_2$H$_6$ ratios could serve as indicator to distinguish microbial from abiotic processes.

Light enhanced the abiotic CH$_4$ formation rates (Fig. 1c) by photolysis of water and generation of H$_2$O$_2$ at 30 °C (Supplementary Fig. 2). Notably, CH$_4$ amounts increased ~4-fold from ~0.02 μM h^{-1} to ~0.08 μM h^{-1} upon broad-spectrum illumination (~350 nm < λ < ~1010 nm at 82 ± 4 μmol photons m^{-2}s^{-1}, Supplementary Fig. 3). This data provides evidence that light-driven CH$_4$ formation from methylated S-compounds can occur even in the absence of biomolecules. The addition of oxygen to the samples stopped the formation of CH$_4$ in this pH-neutral model system supplemented with Fe^{3+} (Fig. 1c). In contrast, under acidic (pH 3), illuminated conditions CH$_4$ formation rates increased ~5-fold upon Fe^{3+}-supplementation in comparison to Fe^{2+}-addition, indicating light-driven ROS and Fe^{2+} formation from [Fe(H$_2$O)$_6$]$^{3+}$ complexes (Fig. 1d)[35]. Upon supplementation of 1 mM Fe^{3+} and 1 mM Fe^{2+}, keeping the overall iron concentration unchanged at 2 mM, CH$_4$ formation rates increased to ~0.33 μM h^{-1}. This 5-fold rate increase is driven by both ROS-inducing Fe^{3+} and Fenton-driving Fe^{2+}. Under pH-neutral conditions, mixing Fe^{2+} and Fe^{3+} only increased CH$_4$ formation rates by ~1.3-fold in comparison to Fe^{2+}-supplemented samples, while only trace amounts of CH$_4$ were obtained from Fe^{3+}-supplemented samples (Supplementary Fig. 4).

Thus, illuminated [Fe(H$_2$O)$_6$]$^{3+}$ complexes generate both Fe^{2+} and ROS, thereby contributing to the ROS-driven CH$_4$ formation under acidic conditions.

Taken together, we demonstrated that heat and light drive the formation of CH$_4$ and C$_2$H$_6$ in an anoxic, abiotic environment under ambient temperatures and pressures. These results establish a ROS-driven mechanism based on Fenton chemistry that can occur delocalized from serpentinization across Earth's humid realm and thereby substantially differs from previously suggested mechanisms that are spatially restricted. Thus, this non-enzymatic hydrocarbon formation mechanism could have released CH$_4$ and C$_2$H$_6$ into the atmosphere of the Hadean and Archean. Besides CH$_4$, C$_2$H$_6$ is considered an important factor in keeping the early Earth warm, since C$_2$H$_6$ absorbs from 11 to 13 μm in an atmospheric window (roughly 8–13 μm) where H$_2$O and CO$_2$ do not absorb strongly[2]. Together, the hydrocarbons produced by these pathways might offer a solution to the "faint young sun paradox"[3,4].

(Bio)molecules enhance the heat-driven CH$_4$ formation

Even before life emerged, several metabolites, e.g. citrate and malate, could have been formed via an ancient, non-enzymatic TCA cycle predecessor driven by ROS[39,40]. Catalyzed by iron particles, the formation of pyruvate from CO$_2$ was recently reported[41]. Intriguingly, citrate and malate, as well as other primordial (bio)molecules with a putative prebiotic origin, including ATP[42] or serine[43], have been reported to act as Fenton-promoting Fe^{2+}-chelators[26]. We therefore investigated if these hydroxylated and carboxylated (bio)molecules enhance the ROS-driven CH$_4$ formation rates (Fig. 2a).

Indeed, the addition of pyruvate, glucose, serine, ATP, malate or citrate to the heat-driven (97 °C) model system increased the abiotic CH$_4$
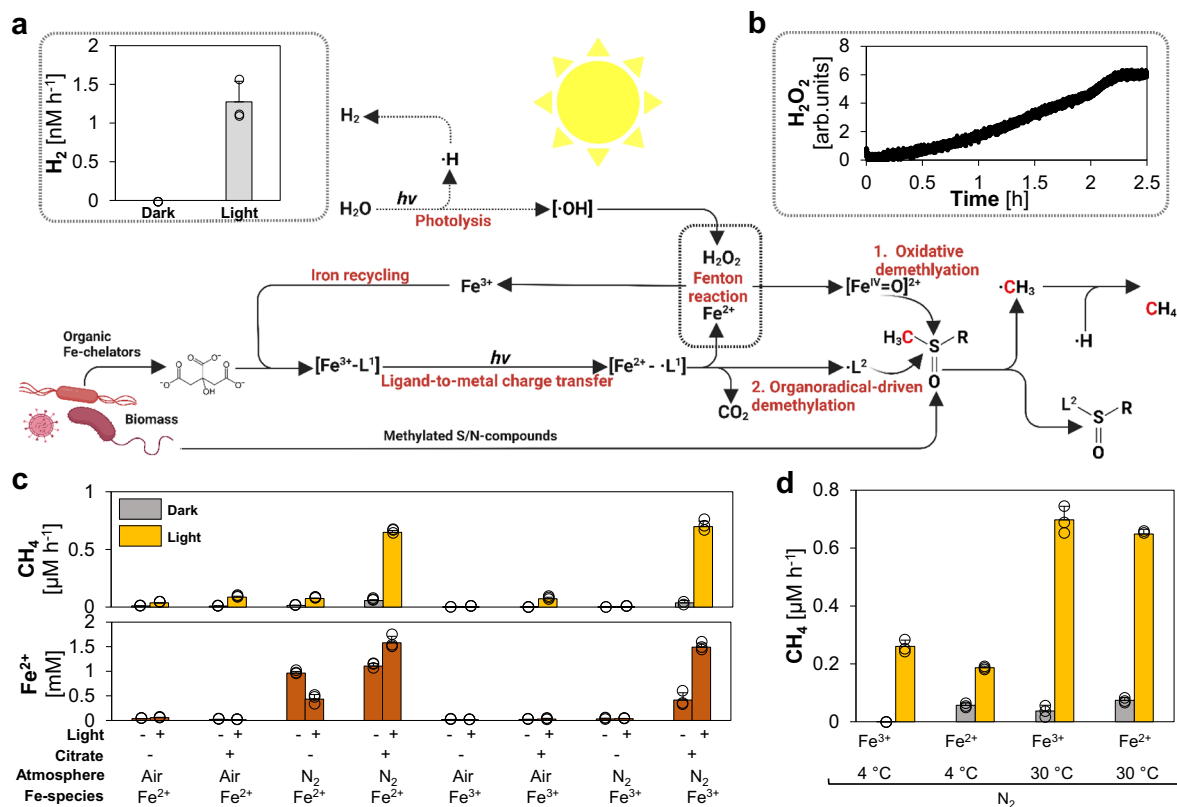
Fig. 3 | A light-driven iron redox cycle drives and enhances CH₄ formation.
Upon illumination, water is photolytically split into hydroxyl radicals (·OH) and hydrogen forming H_2 and H_2O_2. Organic Fe^{3+}-complexes (Fe^{3+}-[L^1]) are converted into Fe^{2+} and organic radicals (·L^1) via ligand-to-metal charge transfer (LMCT). The generated Fe^{2+} reacts with H_2O_2 to ·OH or [Fe^{IV}= O]²⁺ and thereby drives the generation of methyl radicals (·CH_3) from S-/N-methylated compounds. The LMCT-generated ·L^1 decomposes into CO_2 and another organic radical (·L^2) that additionally facilitates CH₄ formation upon reacting with S-/N-methylated compounds. Under light, (**a**) H_2 (gray bars) and (**b**) H_2O_2 is formed in pure buffer. **c** Upon

illumination, CH₄ formation rates (yellow bars) are increased. Fe^{2+} formation (brown bars) depends on anoxic conditions and is driven by LMCT induced by the addition of citrate. **d** Light and heat have synergistic effects on CH₄ formation. While heat drives CH₄ formation upon Fe^{2+}-supplementation, light increases CH₄ formation upon Fe^{3+}- and Fe^{2+}-addition. All experiments were conducted in closed glass vials containing a buffered solution (pH 7) supplemented with DMSO, Fe^{3+} or Fe^{2+}, N_2 or air atmosphere in the presence or absence of citrate incubated under light or in the dark at 4 °C or 30 °C. The bars are the mean + standard deviation of triplicates, shown as circles. **a**, **b** Was created with BioRender.com.

formation rate, e.g. more than 11-fold for citrate (Fig. 2b). Corresponding C_2H_6 rates significantly increased for glucose, serine, malate and citrate, resulting in CH₄:C_2H_6 ratios between ~190 (glucose) and ~1100 (citrate, Fig. 2b). To test if these enhancing effects were indeed driven by Fe^{2+} chelation, we supplemented the assays with the Fe^{2+}-competitor Ca^{2+} (Fig. 2c). Since (bio)molecules like citrate can alternatively chelate Ca^{2+} ions, we expected that increasing Ca^{2+} concentrations result in decreasing CH₄ formation rates by replacing Fenton-promoting Fe^{2+}-citrate complexes with Ca^{2+}-citrate complexes. Upon addition of 10 mM and 500 mM Ca^{2+}, CH₄ formation rates significantly decreased from ~6.32 µM h⁻¹ to ~4.86 µM h⁻¹ and ~1.29 µM h⁻¹, respectively. Thus, 500 mM Ca^{2+} suppressed ~90% of the Fenton-promoting effect of citrate supplementation. The Ca^{2+} concentration-dependent decrease of the heat-driven CH₄ formation rate supports the role of citrate as a Fenton-promoting Fe^{2+}-chelator, which is further indicated by citrate dissolving any ferruginous precipitate.

Together, ROS generated by heat interact with iron and thereby drive the formation of methyl radicals from S-/N-methylated compounds, resulting in CH₄ and C_2H_6. Moreover, several hydroxylated or carboxylated (bio)molecules with a putative prebiotic origin were shown to act as Fenton-promoting Fe^{2+}-chelators, indicating that ROS-driven CH₄ formation may have already been widespread within the timeframe of the transition from prebiotic chemistry to the origin of life. The rise of life would have fostered the abiotic, non-enzymatic CH₄ formation due to the consequential formation and release of biomolecules serving as chelators and substrates.

A light-driven iron redox cycle sustains CH₄ formation

During Fenton chemistry, Fe^{2+} is either oxidized to [Fe^{IV}= O]²⁺ or ferric iron (Fe^{3+}). As Fe^{3+} cannot drive Fenton reactions[23,24], CH₄ formation rates decrease with increasing reaction time and increasing concentrations of Fe^{3+}. While this effect may have been minor in the ferruginous Archean oceans, Fe^{3+} likely dominated the iron pool in the photic zone of the oceans latest by the rise of photoferrotrophy and was also prevalent in several ecological niches, e.g. volcanic lakes[34]. The evolution of photosynthesis and the subsequent biological production of O_2 oxidized the majority of the available Fe^{2+} to Fe^{3+}. Thus, abiotic ROS-driven CH₄ formation would have been hindered in the sunlit realm by the late Archean in the absence of an iron redox cycle at neutral pH. Intriguingly, besides acting as Fenton-promoting Fe^{2+}-chelators[26], (bio)molecules like citrate were reported to reduce Fe^{3+} to Fe^{2+} via LMCT under oxic and anoxic conditions[27]. Therefore, (bio)molecules may have facilitated widespread iron redox cycling, e.g. by forming Fe(III)-carboxylate complexes. Furthermore, previous studies showed that, upon illumination of water hydroxyl radicals (·OH) and hydrogen atoms are generated, forming H_2O_2 and H_2[30–33]. Thus, we hypothesized that light could drive CH₄ formation in the absence of Fe^{2+} by simultaneously (i) generating ROS from water and (ii) reducing Fe^{3+} to Fe^{2+} via LMCT, thereby recycling Fe^{3+} and keeping the Fenton reaction running (Fig. 3).

To verify our hypothesis, we first confirmed light-dependent ROS production in our model system in the absence of substrate, iron and organic ligands by measuring final reaction products of

photolysis: H_2 and H_2O_2 (Fig. 3a, b). We measured H_2 production at a rate of ~1.3 nM h^{-1} in anoxic samples under broad-spectrum illumination but not in samples kept in the dark (Fig. 3a). A continuous formation of H_2O_2 was measured online using microsensors, which confirmed light-dependent production dynamics in pure buffer (Fig. 3b). Via fluorescence-based H_2O_2 endpoint measurements, we found that both iron and DMSO reduced the H_2O_2 concentrations. The decrease in H_2O_2 levels can be attributed to Fenton reactions between H_2O_2, Fe^{2+} and the radical scavenger DMSO (Supplementary Fig. 5).

Building on this, we closely investigated the interplay of LMCT and iron photochemistry on CH_4 formation. For this purpose, we analyzed our chemical model system containing a buffered solution (pH 7), Fe^{2+} or Fe^{3+}, DMSO, in the presence or absence of citrate for the formation of CH_4 and the concentration of available Fe^{2+} (Fig. 3c). The influence of the following parameters on the formation of CH_4 was tested: (i) O_2 (~ 21% in air), (ii) oxidation state of the supplemented iron species (Fe^{2+} vs. Fe^3), (iii) light and (iv) presence/absence of citrate. (i) CH_4 formation rates under anoxic conditions always exceeded rates under oxic conditions. (ii) Without citrate, initial Fe^{2+}-supplementation was required to form significant CH_4 levels. (iii) CH_4 formation always increased with light. (iv) Upon citrate addition, CH_4 formation was enhanced in illuminated and anoxic samples containing DMSO and Fe^{2+} or Fe^{3+}. Besides elevated CH_4 formation rates, citrate addition also increased the final Fe^{2+} concentrations, e.g. from ~0 mM Fe^{2+} to ~1.5 mM Fe^{2+} in illuminated and anoxic samples.

After determining the influence of the four parameters (i) O_2, (ii) iron (iii) light and (iv) (bio)molecules, we further investigated them individually to gain a better understanding of their contribution and role in the light-driven CH_4 formation.

(i) O_2: The influence of O_2 on LMCT and CH_4 formation was studied in citrate-supplemented samples by adding various amounts of air. Fe^{2+} concentrations and CH_4 formation rates decreased with increasing O_2 levels (Supplementary Fig. 6). In comparison to 0 % O_2, the Fe^{2+} concentration dropped drastically already at 0.2 % O_2 and was ~96 % lower at 2 % O_2, while CH_4 formation rates decreased approximately linearly with the O_2 level. This indicates the presence of a Fe-cycle, in which most LMCT-formed Fe^{2+} is instantly re-oxidized, either by O_2 or Fenton reactions. The balance between these Fe^{2+} sinks depend on O_2 availability and governs CH_4 formation rates. In the presence of O_2, we also detected methanol (CH_3OH) formation rates ranging from ~0.003 µM h^{-1} (0.2 % O_2) to ~0.07 µM h^{-1} (21 % O_2). CH_3OH is preferentially formed through the reaction of $\cdot CH_3$ with O_2[23,44]. Without the addition of O_2, no CH_3OH was detected, indicating anoxic conditions in our standard assays.

(ii) Iron: The role of the LMCT-rate and the corresponding Fe^{2+} availability for CH_4 formation was tested by supplementing the assays with various Fe^{3+} concentrations (Supplementary Fig. 7). At lower Fe^{3+} concentrations, CH_4 formation rates increased steeper than the measured Fe^{2+} concentrations. At high Fe^{3+} concentrations, CH_4 formation rates leveled off, while Fe^{2+} concentrations continued to increase. This indicates that Fe^{2+} is limiting the demethylation rates at low iron concentrations, because it is immediately re-oxidized, while light-dependent ROS production is limiting CH_4 formation at high iron concentrations. Most importantly, these data highlight that a light- and ROS-driven iron cycle can facilitate high rates of CH_4 formation, even in the presence of O_2 and the absence of detectable Fe^{2+}, which opens the possibility of widespread abiotic CH_4 production after the great oxidation event as well as in diverse modern habitats. Next, we investigated the role of the alkali metal magnesium (Mg^{2+}) due to its high environmental abundance and found that Mg^{2+} does not facilitate CH_4 formation in illuminated buffer containing DMSO and citrate (Supplementary Fig. 8). Upon additional Fe^{3+} supplementation, Mg^{2+} also decreased CH_4 formation rates by replacing Fenton-promoting

Fe^{3+}-citrate complexes by Mg^{2+}-citrate complexes, thereby acting similar to Ca^{2+} that was demonstrated to decrease heat-driven CH_4 formation (Fig. 2c). Besides iron, the transition metals copper, cerium, cobalt, nickel and manganese were reported to drive Fenton chemistry[45,46], resulting in the release of CH_4. Thus, we tested different transition metals in our chemical model system, containing DMSO as substrate and ascorbate as a strong metal reductant[47,48]. We observed that copper, cobalt and cerium also enhanced CH_4 formation rates (Fig. 4a). However, the activity of copper, cobalt and cerium was lower than iron. The high activity of iron combined with its ubiquitous abundance in the Precambrian highlights the global distribution and importance of this mechanism.

(iii) Light: It is established that light quality has an important influence on photolysis. Short wavelength light in the ultraviolet spectrum was reported to drive water photolysis and LMCT more efficiently than longer wavelengths[49]. We expected that shorter wavelength light would increase both CH_4 formation rates and Fe^{2+} levels. Indeed, CH_4 formation rates surged from ~0.3 µM h^{-1} (λ_{max} = 534 nm) to ~1.23 µM h^{-1} (λ_{max} = 388 nm, Fig. 4b) and Fe^{2+} concentrations almost tripled from ~1.3 mM (λ_{max} = 534 nm) to ~4.2 mM (λ_{max} = 388 nm). Although the broad-spectrum light had a 1.5-fold higher energy flux (57 ± 2 kJ m^{-2} h^{-1}) compared to the 388 nm-LED light (37 ± 2 kJ m^{-2} h^{-1}), the CH_4 formation rate under the broad-spectrum light was only half (0.7 µM h^{-1}). Given that the stratospheric ozone layer was absent during the Hadean and Archaean, higher fluxes of short wavelength light (i.e. ultraviolet light), reached aqueous environments and may have further enhanced the ROS-driven CH_4 formation.

(iv) (Bio)molecules: After illumination of Fe^{3+}-ligand complexes, one electron is transferred via LMCT from a carboxylated ligand (L^1) to Fe^{3+}, an organic radical ($\cdot L^1$), i.e. citrate radical, is generated. As described in the literature[28], we observed the subsequent CO_2 disassembly from citrate radicals (Supplementary Fig. 9). We speculated that the remaining organic radical ($\cdot L^2$) could react with DMSO, resulting in $\cdot CH_3$ and the formation of CH_4 (Fig. 3). Since we cannot directly detect organic radicals, we mimicked the proposed reaction in an anoxic model system only containing DMSO and the radical-generating 2,2'-azobis(2-amidinopropane) dihydrochloride (APPH) that readily decomposes into carbon-centered organic radicals at 40 °C (Supplementary Fig. 10). Indeed, we observed CH_4 formation in a mixture of DMSO and APPH, while only trace amounts of CH_4 were observed from either DMSO or AAPH alone, suggesting an organic radical-driven CH_4 formation mechanism. In short, carboxylates like citrate facilitate LMCT, thereby reducing Fe^{3+} to Fe^{2+} and forming organic radicals. Both resulting compounds drive CH_4 formation. Overall, CH_4 can be formed under anoxic conditions via (i) water thermolysis, (ii) water photolysis, (iii) $[Fe(H_2O)_6]^{3+}$ photolysis and (iv) LMCT-induced carbon-centered radicals. Apart from serving as chelators, some (bio)molecules could also serve as substrates for Fenton reactions. Thus, we investigated four S-/N-methylated compounds in the presence of the chelator citrate. Upon illumination, CH_4 was formed from dimethyl sulfide, methionine, 2-methylthioethanol and trimethylamine (Fig. 4c). These observations indicate that ROS-driven CH_4 formation significantly increased after the origin of life by providing biomolecules as chelators and substrates.

Finally, synergistic effects between light and heat were observed (Fig. 3d). For Fe^{2+}-supplemented samples, CH_4 rates at 4 °C increased from ~0.056 µM h^{-1} in the dark over ~0.19 µM h^{-1} under light to ~0.65 µM h^{-1} in illuminated samples at 30 °C. For Fe^{3+}-supplemented samples, only CH_4 rates below 0.03 µM h^{-1} were obtained in the dark, while CH_4 formation rates were slightly above Fe^{2+}-supplemented samples in the light, again demonstrating the effects of LMCT and LMCT-induced carbon-centered radicals. Thus, the two factors heat and light synergistically combine for a stable and enhanced ROS and CH_4 formation.
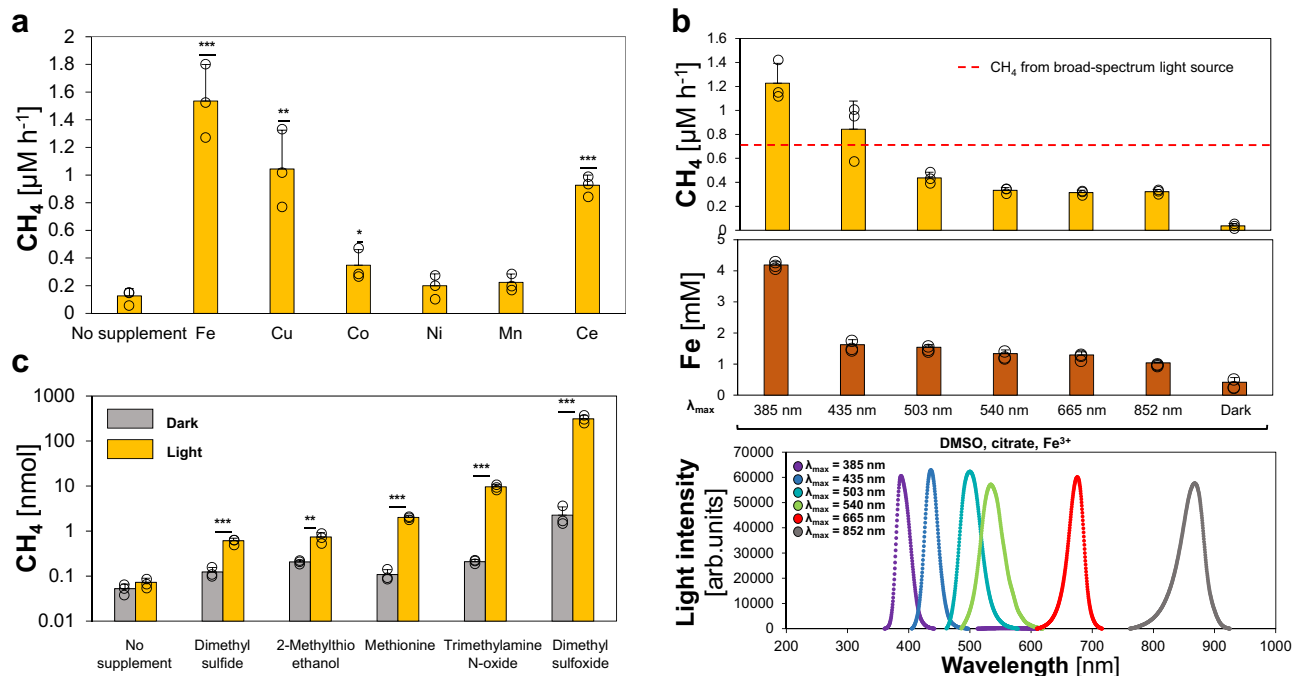
Fig. 4 | Transition metals, wavelengths and methylated sulfur- and nitrogen compounds mediate light-driven CH$_4$ formation. a Iron, cobalt and cerium enhance light-driven CH$_4$ formation. No significant CH$_4$ increase was observed for cobalt, nickel and manganese supplementation. **b** Light-driven CH$_4$ formation and Fe^{2+} generation increases in the near-UV spectrum. **c** Light-driven formation of CH$_4$ from methylated S-/N-compounds (logarithmic scale). Upon illumination, significant increases in CH$_4$ levels were measured for dimethyl sulfide, methionine, 2-methylthioethanol, trimethylamine N-oxide and dimethyl sulfoxide (DMSO). All experiments were conducted in closed glass vials containing a buffered solution (pH 7), N$_2$ and either Fe^{3+} or other transition metals (**a**), DMSO or other substrates (**c**) and either ascorbate (**a**) or citrate (**b, c**). Samples were incubated under broad-spectrum light (**a, c**), specific wavelengths (**b**) or in the dark at 30 °C. The dashed red line depicts the average CH$_4$ amounts obtained from samples illuminated by a broad-spectrum light source. Statistical analysis was performed using paired two-tailed t tests, *$p \leq 0.05$, **$p \leq 0.01$, ***$p \leq 0.001$. The bars are the mean + standard deviation of triplicates, shown as circles.
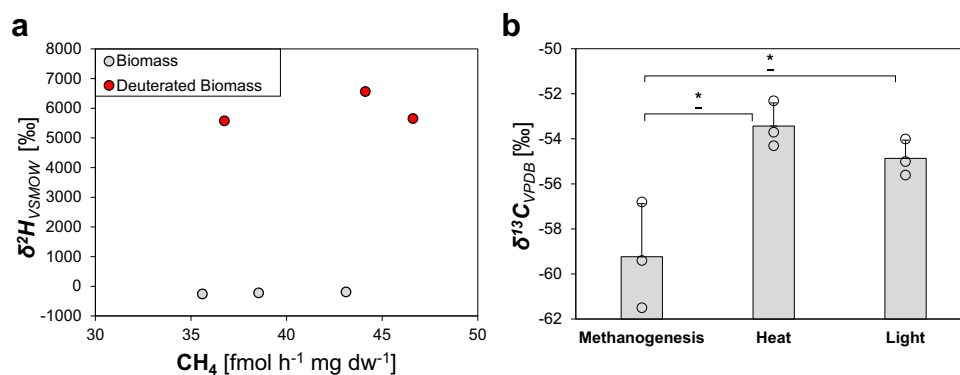

Fig. 5 | Isotope labeling studies confirm dead biomass as substrate and show an abiotic isotope fractionation for ROS-driven CH$_4$ formation. a Unlabeled or deuterium-enriched CH$_4$ is formed from unlabeled biomass (gray dots) or deuterated biomass (red dots), respectively. **b** Stable carbon isotope values of cultures from the methanogen *Methanothermobacter marburgensis*, heat-, or light-generated CH$_4$. All experiments were conducted in closed glass vials containing a buffered solution (**a, b**−heat, light) or culture medium (**b**−methanogenesis), supplemented with Fe^{3+} and ascorbate (**a**) or Fe^{2+} and citrate (**b**−heat, light) under a nitrogen atmosphere, incubated under light at 30 °C or in the dark at 97 °C. Statistical analysis was performed using paired two-tailed t tests, *$p \leq 0.05$. The bars are the mean + standard deviation of triplicates, shown as circles.

Biomass-derived CH$_4$ with an abiotic isotope fractionation

Considering the impact of (bio)molecules on the LMCT-driven Fenton reaction, organic radical generation and the role of biomolecules as substrates, we expect the discussed mechanisms to have played and still play the most important role in the vicinity of decaying biomass. To demonstrate that CH$_4$ is indeed formed from dead biomass in the presence of a variety of biomolecules and not just in our well-defined model systems, we conducted deuterium labeling experiments. For this purpose, we grew the bacterium *B. subtilis* in *Luria-Bertani*

medium supplemented with 10% D$_2$O and inactivated the cells by sonication and freezing (see Methods).

The obtained dead biomass was supplemented with Fe^{3+} and ascorbate and incubated under broad-spectrum light. Around 40 fmol CH$_4$ h^{-1} mg^{-1} dry weight was obtained from labeled and unlabeled biomass (Fig. 5a). In addition, stable hydrogen isotope values ($\delta^2 H$) of CH$_4$ from D$_2$O-treated biomass showed strong enrichment in deuterium (~5900 ‰) in comparison to unlabeled biomass (~−225 ‰), demonstrating a direct conversion of isotopically labeled biomass to

CH_4. This suggests that the availability of biomass, upon the emergence of life, has increased the CH_4 formation by delivering both (i) S-/N-methylated compounds and (ii) Fenton-promoting iron chelators. The presence of CH_4 has been suggested to be crucial for the evolution of life, since it could serve as life´s first carbon source via methanotrophy[50–52]. Following this line of thought, we could demonstrate that methanotrophic *Methylocystis hirsuta* grew on CH_4 generated by our light-driven model system, transferred to the headspace of the *M. hirsuta* culture (Supplementary Fig. 11). In fact, the "last methane-metabolizing ancestor" had likely the genes to perform methanogenesis and anaerobic methane oxidation[53], suggesting that, under high CH_4 concentrations, methanotrophy could have emerged prior to methanogenesis.

Finally, we speculated that ROS-driven CH_4 formation leads to different stable carbon isotope values ($\delta^{13}C$) compared to biological processes, *i.e.*, methanogenesis. The observed $\delta^{13}C$ values for CH_4 generated by heat or light were less negative ($-\sim54 \pm 1.1‰$) compared to the $\delta^{13}C$ value of the methanogen *Methanothermobacter marburgensis* ($-\sim59.2 \pm 2.3‰$, Fig. 5b). While the isotopic fractionation during abiotic ROS-driven CH_4 formation remains to be studied in depth, these results suggest a lower carbon isotope fractionation for ROS-driven CH_4 formation than for enzymatic methanogenesis. Together with the observed $CH_4:C_2H_6$ ratios, isotopic signatures may therefore serve to differentiate between CH_4 formed enzymatically or abiotically on Earth and extraterrestrial planets.

Discussion

In this work, we demonstrated that the interplay of Fe^{2+} and H_2O_2, generated by heat and light, drives CH_4 and C_2H_6 formation from methylated S-/N-compounds via Fenton chemistry under conditions that were globally prevalent in the Hadean and Archean. As we observed CH_4 formation under suboxic and oxic conditions, these mechanisms could, in principle, also contribute to extant CH_4 emissions from aqueous environments that were recently shown to correlate with light instead of specific enzymatic pathways[54]. The here described pathways allow CH_4 and C_2H_6 formation in many aqueous environments including oceans, lakes, rivers, and ponds, delocalized from restricted hotspots for (bio)molecule formation such as hydrothermal vents or ultramafic rocks, in superficial water layers driven by light and throughout the entire water column driven by heat. After the emergence of life, this phenomenon would have greatly intensified in the anoxic Archaean and the subsequent "boring billion"[55,56]. The increasing amounts of biomass provided methylated S-/N-substrates, Fe-chelating biomolecules reducing Fe^{3+} to Fe^{2+} and releasing organic radicals and thus enhance ROS-driven CH_4 formation. Possibly, these reactions facilitated elevated CH_4 and C_2H_6 levels during the Hadean and Archean. These hydrocarbons would have contributed to atmospheric temperatures on Earth and allowed the evolution of life in a liquid hydrosphere which could have influenced the evolution of metabolism by allowing the rise of methanotrophy prior to methanogenesis. This work lays the foundation to explore further the mechanism's role in shaping the evolution of the atmosphere on Earth and other planets and its influence on the current climate change.

Methods

General assay conditions
Unless otherwise indicated, 4 mL samples were incubated in closed 20 mL glass vials at 30 °C under a pure nitrogen (N_2) atmosphere and subsequently analyzed via gas chromatography (GC).

Heat assays
In total, 500 mM DMSO and 10 mM $FeSO_4$ were added to 20 mM degassed potassium phosphate buffer (pH 7) in an anaerobic tent. The headspace of the closed vials was then cycled three times with vacuum and N_2. Samples were incubated at 37 °C, 57 °C, 77 °C and 97 °C for 6 h

in an incubator in the dark. Optionally, 20 mM citrate, malate, ATP, serine, glucose or pyruvate were also supplemented. Ca^{2+} was added in the form of $CaCl_2$. Samples were measured within the linear range of CH_4 formation rate via gas chromatography.

Light assays
In total, 500 mM DMSO, 2 mM of either $FeCl_3$ or $FeSO_4$ and, optionally, 10 mM citrate were added to 20 mM degassed potassium phosphate buffer (pH 7). Anoxic conditions were generated by drawing vacuum eight times for 1 min and a subsequent filling with N_2. For experiments investigating $[Fe(H_2O)_6]^{3+}$ complexes, samples were incubated under anoxic, acidic conditions (20 mM Tris · HCl buffer, pH 3) and supplemented with 500 mM DMSO and either 2 mM $FeCl_3$, 2 mM $FeSO_4$ or 1 mM $FeCl_3$ and 1 mM $FeSO_4$, each. For the investigation of transition metals (Fig. 4a), 2 mM cerium ($CeNH_4SO_4$), manganese ($MnSO_4$), cobalt ($CoNO_3$), nickel ($NiSO_4$), copper ($CuCl_2$) or iron ($FeCl_3$) and 10 mM pH-neutral ascorbate were added to 500 mM DMSO and 20 mM potassium phosphate buffer with an incubation for 1 day. The effect of different wavelengths on CH_4 formation (Fig. 4b) was investigated by adding 5 mM $FeCl_3$, 10 mM citrate and 500 mM DMSO to 20 mM potassium phosphate buffer with an incubation for 1 day. For the determination of substrates for CH_4 formation (Fig. 4c), 500 mM DMS, methionine, 2-methylthioethanol, Trimethylamine N-oxide or DMSO were added to 10 mM $FeCl_3$ and 100 mM citrate in 20 mM potassium phosphate buffer with an incubation for 3 days. Samples were incubated under air or N_2 in the dark or under constant broad-spectrum illumination from light bulbs (Osram, Superlux, Super E SIL 60; $\Phi = 82 \pm 4$ µmol photons m^{-2} s^{-1}, $H = 52 \pm 2$ kJ m^{-2} h^{-1}; Supplementary Fig. 3) for 1 day. Samples were measured within the linear range of the CH_4 formation via gas chromatography. Specific wavelengths were provided by diodes (H2A1 series, Roithner Lasertechnik, Austria) emitting UV-A, blue, cyan, green, red or near-infrared light ($\lambda_{max} = 388$ nm, $\Phi = 35 \pm 1$ µmol photons m^{-2} s^{-1}; $H = 36 \pm 2$ kJ m^{-2} h^{-1}; $\lambda_{max} = 436$ nm, $\Phi = 45 \pm 1$ µmol photons m^{-2} s^{-1}, $H = 45 \pm 1$ kJ m^{-2} h^{-1}; $\lambda_{max} = 500$ nm, $\Phi = 64 \pm 4$ µmol photons m^{-2} s^{-1}, $H = 55 \pm 3$ kJ m^{-2} h^{-1}; $\lambda_{max} = 534$ nm, $\Phi = 63 \pm 1$ µmol photons m^{-2} s^{-1}, $H = 50 \pm 1$ kJ m^{-2} h^{-1}; $\lambda_{max} = 675$ nm, $\Phi = 45 \pm 4$ µmol photons m^{-2} s^{-1}, $H = 29 \pm 3$ kJ m^{-2} h^{-1}; or $\lambda_{max} = 868$ nm, $\Phi = 69 \pm 7$ µmol photons m^{-2} s^{-1}, $H = 35 \pm 3$ kJ m^{-2} h^{-1}) Light intensity was determined using a fiber optic scalar irradiance microsensor[57] connected to a spectrometer (USB4000; Ocean Optics, USA) placed in the center of the incubation vials and calibrated using a spherical light probe (Walz) connected to a LI-250A light meter (Li-Cor Biosciences GmbH, Germany)[58]. Concentration of Fe^{2+} was quantified with the colorimetric ferrozine method[59].

Bacillus subtilis biomass assays
B. subtilis was grown in 500 mL LB media, supplemented with 10 % H_2O or D_2O, grown for 36 h at 37 °C and 180 rpm. The obtained culture was collected by three cycles of centrifugation (10 min, $4743 \times g$) and resuspended in 35 mL 20 mM potassium phosphate buffer (pH 7) in order to remove the excess D_2O. Biomass was then generated by sonication (4-times, 1 min) and freezing of the samples. Subsequently, 80 mL buffer was supplemented with 10 mL biomass, 20 mM $FeCl_3$ and 50 mM ascorbic acid, saturated with N_2 for 30 min and incubated in 100 mL closed glass vials under N_2 and constant broad-spectrum illumination for 3 days. The gas headspace was extracted with a syringe and analyzed with regard to CH_4 content and δ^2H values.

Methylocystis hirsuta and Methanothermobacter marburgensis cultivation
M. hirsuta growth media contained 0.5 g $Na_2HPO_4 \cdot 2H_2O$, 0.22 g KH_2PO_4, 1 g KNO_3, 0.4 mg $CaCl_2 \cdot 2H_2O$, 2 mg $MgSO_4 \cdot 7H_2O$ per liter, supplemented with 5 mg Na_2EDTA, 0.06 mg $CuCl_2 \cdot 5H_2O$, 2 mg $FeSO_4 \cdot 7H_2O$, 0.1 mg $ZnSO_4 \cdot 7H_2O$, 0.03 mg $MnCl_4 \cdot 4H_2O$, 0.05 mg H_3BO_3, 0.2 mg $CoCl_2 \cdot 6H_2O$, 0.02 mg $NiCl_2 \cdot 6H_2O$ and 0.03 mg $Na_2MoO_4 \cdot 2H_2O$

per liter. *M. hirsuta* was cultivated in 100 mL closed glass vials containing 30 mL culture and was incubated at 25 °C and 150 rpm under an air atmosphere. Methane was produced by supplementing 2 L degassed 20 mM potassium phosphate buffer with 1 M DMSO, 25 mM $FeSO_4$ and 50 mM ascorbic acid, incubating the solution under constant illumination in 1 L flasks and collecting the formed CH_4 with syringes. *M. hirsuta* cultures were either supplemented with 25 mL light-generated CH_4 or 25 mL pure N_2. *M. marburgensis* was cultivated as previously described[60].

Continuous H_2O_2 measurements using microsensors

To visualize H_2O_2 production in the illuminated anoxic model system, an H_2O_2 microsensor was positioned in the solution. The H_2O_2 microsensors were built, calibrated and used as described previously[61]. We sealed the vial opening with self-adhesive tape, rigorously bubbled the liquid with N_2 and then adjusted a gentle flow of N_2 through the headspace to minimize oxygen input from the atmosphere. Light was provided from halogen lamps (KL2500, Schott) at an intensity of 1027 μmol photons m^{-2} s^{-1}. We did not attempt to calculate light-dependent H_2O_2 production rates due to the open design of the system, which allowed for the exchange of H_2O_2 with the headspace across the water interface.

End-point H_2O_2 measurements

After illumination, 290 μL sample was mixed anaerobically with 9 μL Amplex Ultrared (Thermofisher, A36006, 30 μM final concentration) and 1 μL recombinant APEX2 (0.23 μM final concentration). Fluorescence was then measured with a plate reader (BMG ClarioStar™) at 568 nm excitation / 581 nm emission. A calibration curve was established with H_2O_2 following the same procedure. To prevent O_2-driven H_2O_2 generation while sample preparation, all buffers were saturated with N_2 and the plate reader was kept at a partial oxygen pressure of 0.1% with an atmospheric control unit (Clariostar, BMG). Before sample preparation, all sample components (20 mM potassium phosphate buffer, DMSO, 1 M citrate and 100 mM $FeCl_3$) were degassed and kept in an anoxic tent overnight.

Quantification of CH_4, C_2H_6, CO_2, and H_2 (GC-FID)

Amounts of formed CH_4, C_2H_6, CO_2 and H_2 were determined via headspace analysis using a PerkinElmer® Clarus®690 GC system (GC–FID/TCD) with a custom-made column circuit (ARNL6743). The headspace samples were injected by a TurboMatrixX110 (PerkinElmer Inc, Waltham, USA) autosampler, heating the samples to 45 °C for 15 min prior to injection. The samples were then separated on a HayeSep column (7′ HayeSep N 1/8″ Sf; PerkinElmer®), followed by molecular sieve (9′ Molecular Sieve 13×1/8″ Sf; PerkinElmer®) kept at 60 °C. Subsequently, the gases were detected with a flame ionization detector (FID, at 250 °C) and a thermal conductivity detector (TCD, at 200 °C). The quantification of CH_4, C_2H_6, CO_2 and H_2 was based on linear standard curves that were derived from measuring varying amounts of these gases.

CH_3OH measurements (GC-FID)

CH_3OH was quantified with a GC-FID (Shimadzu GC-2010 Plus, FID-2010 Plus, 280 °C) containing an AOC 20i autosampler and a ZB-WAXplus (Zebron) column (30 m x ⌀ = 0.25 mm, df, 0.25 μm). A H_2O sample (1 μL) was injected in the split liner (250 °C, split 5,15,50). The temperature program was kept at 35 °C for 5 min and then increased by 50 °C min^{-1} until 200 °C which was kept for 3 min. Helium served as carrier gas (flow rate: 1.95 ml min^{-1}) and the FID was operated with 400 ml min^{-1} synthetic air, 40 ml min^{-1} H_2 and 30 ml min^{-1} N_2, serving as a makeup gas. For Split 5, a calibration curve (R^2 = 0.9931) was generated by diluting CH_3OH (99.9% purity), while an R^2 = 0.9981 for split 15 and an R^2 = 0.9997 for split 50 was determined.

δ ^{13}C stable isotope measurements (GC-C-IRMS)

$\delta^{13}C$ values of CH_4 were determined by gas chromatography-combustion-isotope ratio mass spectrometry (GC-C-IRMS). Aliquots of headspace gas were transferred to an evacuated sample loop (40 mL) and a cryogenic pre-concentration unit to trap CH_4. CH_4 was trapped on HayeSep D, separated from interfering compounds by GC and transferred to the GC-C-IRMS. The system consists of a cryogenic pre-concentration unit directly connected to an HP 6890 N GC (He flow rate: 1.8 mL min^{-1}; Agilent Technologies, Santa Clara, USA) fitted with a GS-Carbonplot capillary column (30 m * 0.32 mm i.d., d_f 1.5 μm; Agilent Technologies) and a PoraPlot capillary column (25 m * 0.25 mm (i.d.), d_f 8 μm; Varian, Lake Forest, USA). The GC flow was coupled using a press-fit connector to a combustion reactor comprised of an oxidation reactor (ceramic tube (Al_2O_3), length 320 mm, inner diameter 0.5 mm, with oxygen-activated Cu/Ni/Pt wires inside; reactor temperature 960 °C) and a GC Combustion III Interface (ThermoQuest Finnigan) to decompose CH_4 into CO_2. $^{13}C/^{12}C$ ratios were determined with a Delta^{PLUS}XL mass spectrometer (ThermoQuest Finnigan, Bremen, Germany). High-purity CO_2 (Messer Griesheim, Frankfurt, Germany) was used as the working monitoring gas. $^{13}C/^{12}C$ ratios ($\delta^{13}C$ values) are expressed in the conventional δ notation in per mil versus VPDB, calculated as:

$$\delta^{13}C_{VPDB} = \left(\frac{\left(\frac{13C}{12C}\right)_{Sample}}{\left(\frac{13C}{12C}\right)_{Standard}} \right) - 1 \tag{1}$$

$\delta^{13}C$ values were corrected using three reference standards of high-purity CH_4 with $\delta^{13}C$ values of −54.5 ± 0.2 ‰ (Isometric Instruments, Victoria, Canada), −66.5 ± 0.2 ‰ (Isometric Instruments) and −42.3 ± 0.2 ‰ (in-house), calibrated against International Atomic Energy Agency and NIST reference substances.

δ^{2}H stable isotope measurements (GC-TC-IRMS)

δ^2H values for CH_4 were determined using GC-temperature conversion-isotope ratio mass spectrometry (GC-TC-IRMS). The analytical set-up was the same as the one used for $\delta^{13}C$ stable isotope measurements except that the He flow rate was changed to 0.6 ml min^{-1} and, instead of combustion to CO_2 and H_2O, CH_4 was thermolytically converted (at 1450 °C) to hydrogen and carbon. After IRMS measurements, the obtained δ^2H values were corrected by using two reference standards of high-purity CH_4 with δ^2H values of −149.9‰ ± 0.2‰ (T-iso2, Isometric Instruments) and −190.6‰ ± 0.2‰ (in house). All δ^2H values are expressed in the conventional δ notation in per mil versus Vienna Standard Mean Ocean Water (VSMOW), calculated as

$$\delta^2H_{VSMOW} = \left(\frac{\left(\frac{2H}{1H}\right)_{Sample}}{\left(\frac{2H}{1H}\right)_{Standard}} \right) - 1 \tag{2}$$

Statistics

Unless indicated otherwise, all experiments were performed with N = 3 replicates (3 biological replicates). To test for significant differences in CH_4 formation between two samples, single-factor analysis (two-tailed students t test) of variance (ANOVA) was used.

Data availability

References

1. Badr, O., Probert, D. & O'callaghan, P. W. Atmospheric methane: Its contribution to global warming. *Appl. Energy.* **40**, 273–313 (1991).

2. Haqq-Misra, J. D., Domagal-Goldman, S. D., Kasting, P. J. & Kasting, J. F. A revised, hazy methane greenhouse for the Archean Earth. *Astrobiology.* **8**, 1127–1137 (2009).

3. Catling, D. C. & Zahnle, K. J. The Archean atmosphere. *Sci. Adv.* **6**, eaax1420 (2020).

4. Feulner, G. The faint young Sun problem. *Rev. Geophys.* **50**, RG2006 (2012).

5. Kasting, J. F. Atmospheric composition of Hadean–early Archean Earth: The importance of CO. *Geol. Soc. Am. Spec. Pap.* **504**, 19–28 (2014).

6. Wolfe, J. M. & Fournier, G. P. Horizontal gene transfer constrains the timing of methanogen evolution. *Nat. Ecol. Evol.* **2**, 897–903 (2018).

7. Kharecha, P., Kasting, J. & Siefert, J. A coupled atmosphere-ecosystem model of the early Archean earth. *Geobiology.* **3**, 53–76 (2005).

8. Stüeken, E. E. & Buick, R. Environmental control on microbial diversification and methane production in the Mesoarchean. *Precambrian Res.* **304**, 64–72 (2018).

9. Zahnle, K., Claire, M. & Catling, A. D. The loss of mass-independent fractionation in sulfur due to a Palaeoproterozoic collapse of atmospheric methane. *Geobiology.* **4**, 271–283 (2006).

10. Zahnle, K. J., Gacesa, M. & Catling, D. C. Strange messenger: A new history of hydrogen on Earth, as told by Xenon. *Geochim. Cosmochim. Acta.* **244**, 56–85 (2019).

11. Ernst, L. et al. Methane formation driven by reactive oxygen species across all living organisms. *Nature.* **603**, 482–487 (2022).

12. Bižić, M. et al. Aquatic and terrestrial cyanobacteria produce methane. *Sci. Adv.* **6**, eaax5343 (2020).

13. Klintzsch, T. et al. Methane production by three widespread marine phytoplankton species: Release rates, precursor compounds, and potential relevance for the environment. *Biogeosciences.* **16**, 4129–4144 (2019).

14. Hartmann, J. F. et al. High spatiotemporal dynamics of methane production and emission in oxic surface water. *Environ. Sci. Technol.* **54**, 1451–1463 (2020).

15. Lenhart, K. et al. Evidence for methane production by saprotrophic fungi. *Nat. Commun.* **3**, 1–8 (2012).

16. Keppler, F., Hamilton, J. T. G., Braß, M. & Röckmann, T. Methane emissions from terrestrial plants under aerobic conditions. *Nature.* **439**, 187–191 (2006).

17. Rogers, K. L. & Schulte, M. D. Organic sulfur metabolisms in hydrothermal environments. *Geobiology.* **10**, 320–332 (2012).

18. Zeng, X., Alain, K. & Shao, Z. Microorganisms from deep-sea hydrothermal vents. *Mar. Life sci. Technol.* **3**, 204–230 (2021).

19. Duperron, S. et al. The bacterial symbionts of closely related hydrothermal vent snails with distinct geochemical habitats show broad similarity in chemoautotrophic gene content. *Front. Microbiol.* **10**, 1818 (2019).

20. Zherebker, A. et al. Speciation of organosulfur compounds in carbonaceous chondrites. *Sci. Rep.* **11**, 1–13 (2021).

21. Vogt, M., Hopp, J., Gail, H.-P., Ott, U. & Trieloff, M. Acquisition of terrestrial neon during accretion—A mixture of solar wind and planetary components. *Geochim. Cosmochim. Acta.* **264**, 141–164 (2019).

22. Dunbar, K. L., Scharf, D. H., Litomska, A. & Hertweck, C. Enzymatic carbon-sulfur bond formation in natural product biosynthesis. *Chem. Rev.* **117**, 5521–5577 (2017).

23. Althoff, F. et al. Abiotic methanogenesis from organosulphur compounds under ambient conditions. *Nat. Commun.* **5**, 4205 (2014).

24. Enami, S., Sakamoto, Y. & Colussi, A. J. Fenton chemistry at aqueous interfaces. *Proc. Natl. Acad. Sci. USA* **111**, 623–628 (2014).

25. Dodd, M. S. et al. Abiotic anoxic iron oxidation, formation of Archean banded iron formations, and the oxidation of early Earth. *Earth Planet Sci. Lett.* **584**, 117469 (2022).

26. Rush, J. D. & Koppenol, W. H. Reactions of Fe(II)-ATP and Fe(II)-citrate complexes with t-butyl hydroperoxide and cumyl hydroperoxide. *FEBS Lett.* **275**, 114–116 (1990).

27. Lueder, U., Jørgensen, B. B., Kappler, A. & Schmidt, C. Photochemistry of iron in aquatic environments. *Environ. Sci. Process. Impacts.* **22**, 12–24 (2020).

28. Glebov, E. M. et al. Intermediates in photochemistry of Fe(III) complexes with carboxylic acids in aqueous solutions. *Photochem. Photobiol. Sci.* **10**, 425–430 (2011).

29. Bruskov, V. I., Masalimov, Z. K. & Chernikov, A. V. Heat-induced generation of reactive oxygen species in water. *Dokl. Biochem. Biophys.* **384**, 181–184 (2002).

30. Chang, Y. et al. Water photolysis and its contributions to the hydroxyl dayglow emissions in the atmospheres of Earth and Mars. *J. Phys. Chem.* **11**, 9086–9092 (2020).

31. Jin, F., Wei, M., Liu, C. & Ma, Y. The mechanism for the formation of OH radicals in condensed-phase water under ultraviolet irradiation. *Phys. Chem. Chem. Phys.* **19**, 21453–21460 (2017).

32. Azrague, K. et al. Hydrogen peroxide evolution during V-UV photolysis of water. *Photochem. Photobiol. Sci.* **4**, 406–408 (2005).

33. Boyle, J. W., Ghormley, J. A., Hochanadel, C. J. & Riley, J. F. Production of hydrated electrons by flash photolysis of liquid water with light in the first continuum. *J. Phys. Chem.* **73**, 2886–2890 (1969).

34. Agangi, A., Hofmann, A., Ossa Ossa, F., Paprika, D. & Bekker, A. Mesoarchaean acidic volcanic lakes: A critical ecological niche in early land colonisation. *Earth Planet Sci Lett.* **556**, 116725 (2021).

35. Timoshnikov, V. A., Kobzeva, T. V., Polyakov, N. E. & Kontoghiorghes, G. J. Inhibition of Fe^{2+}- and Fe^{3+}- induced hydroxyl radical production by the iron-chelating drug deferiprone. *Free Radic. Biol. Med.* **78**, 118–122 (2015).

36. Benckelberg, H. & Warneck, P. Photodecomposition of Iron(III) hydroxo and sulfato complexes in aqueous solution: wavelength dependence of OH and SO_4-Quantum Yields. *J. Phys. Chem.* **99**, 5214–5221 (1995).

37. Krissansen-Totton, J., Arney, G. N. & Catling, D. C. Constraining the climate and ocean pH of the early Earth with a geological carbon cycle model. *Proc. Natl. Acad. Sci. U.S.A.* **115**, 4105–4110 (2018).

38. Bernard, B. B., Brooks, J. M. & Sackett, W. M. Natural gas seepage in the Gulf of Mexico. *Earth Planet. Sci. Lett.* **31**, 48–54 (1976).

39. Keller, M. A., Kampjut, D., Harrison, S. A. & Ralser, M. Sulfate radicals enable a non-enzymatic Krebs cycle precursor. *Nat. Ecol. Evol.* **1**, 83 (2017).

40. Kitadai, N., Kameya, M. & Fujishima, K. Origin of the reductive tricarboxylic acid (rTCA) cycle-type CO_2 fixation: A Perspective. *Life* **7**, 39–54 (2017).

41. Varma, S. J., Muchowska, K. B., Chatelain, P. & Moran, J. Native iron reduces CO_2 to intermediates and end-products of the acetyl-CoA pathway. *Nat. Ecol. Evol.* **2**, 1019–1024 (2018).

42. Chu, X. Y., Xu, Y. Y., Tong, X. Y., Wang, G. & Zhang, H. Y. The legend of ATP: From origin of life to precision medicine. *Metabolites.* **12**, 461 (2022).

43. Kebukawa, Y., Asano, S., Tani, A., Yoda, I. & Kobayashi, K. Gamma-ray-induced amino acid formation in aqueous small bodies in the early solar system. *ACS Cent. Sci.* **2022**, 1664–1671 (2022).

44. Benzing, K., Comba, P., Martin, B. & Pokrandt, B. bF. Keppler, Non-heme iron-oxo-catalyzed methane formation from methyl thioethers: Scope, mechanism, and relevance for natural systems. *Chem. Eur. J.* **23**, 10465–10472 (2017).

45. Bokare, A. D. & Choi, W. Review of iron-free Fenton-like systems for activating H_2O_2 in advanced oxidation processes. *J Hazard. Mater.* **275**, 121–135 (2014).

46. Hussain, S., Aneggi, E. & Goi, D. Catalytic activity of metals in heterogeneous Fenton-like oxidation of wastewater contaminants: a review. *Environ. Chem. Lett.* **19**, 2405–2424 (2021).

47. Foyer, C. H. & Noctor, G. Ascorbate and glutathione: The heart of the redox hub. *Plant Physiol*. **155**, 2–18 (2011).

48. Oikawa, S. & Kawanishi, S. Distinct mechanisms of site-specific DNA damage induced by endogenous reductants in the presence of iron(III) and copper(II). *Biochim. Biophys. Acta Gene Regul. Mech*. **1399**, 19–30 (1998).

49. Lueder, U., Jorgensen, B., Maisch, M., Schmidt, C. & Kappler, A. Influence of Fe(III) source, light quality, photon flux and presence of oxygen on photoreduction of Fe(III)-organic complexes – Implications for light-influenced coastal freshwater and marine sediments. *Sci. Total Environ*. **814**, 152767 (2022).

50. Russell, M. J. & Nitschke, W. Methane: Fuel or exhaust at the emergence of life? *Astrobiology*. **17**, 1053–1066 (2017).

51. Nitschke, W. & Russell, M. J. Beating the acetyl coenzyme A-pathway to the origin of life. *Philos. Trans. R. Soc. Lond. B, Biol. Sci*. **368**, 20120258 (2013).

52. Ettwig, K. F. et al. Nitrite-driven anaerobic methane oxidation by oxygenic bacteria. *Nature*. **464**, 543–548 (2010).

53. Adam, P. S., Kolyfetis, G. E., Bornemann, T. L. V., Vorgias, C. E. & Probst, A. J. Genomic remnants of ancestral methanogenesis and hydrogenotrophy in Archaea drive anaerobic carbon cycling. *Sci. Adv*. **8**, eabm9651 (2022).

54. Ordóñez, C. et al. Evaluation of the methane paradox in four adjacent pre-alpine lakes across a trophic gradient. *Nat. Commun*. **14**, 2165 (2023).

55. Canfield, D. E. A new model for Proterozoic ocean chemistry. *Nature*. **396**, 450–453 (1998).

56. Canfield, D. E. et al. Ferruginous conditions dominated later neoproterozoic deep-water chemistry. *Science*. **321**, 949–952 (2008).

57. Lassen, C., Ploug, H. & Jørgensen, B. B. A fibre-optic scalar irradiance microsensor: application for spectral light measurements in sediments. *FEMS Microbiol. Lett*. **86**, 247–254 (1992).

58. Klatt, J. M. et al. Anoxygenic photosynthesis controls oxygenic photosynthesis in a cyanobacterium from a sulfidic spring. *Appl. Environ. Microbiol*. **81**, 2025–2031 (2015).

59. S. S. Nielsen, C. E. Carpenter, R. E. Ward Eds., Iron Determination by Ferrozine Method. *Food analysis laboratory manual*. 157–159 (Springer, 2017).

60. Vitt, S. et al. The F420-reducing [NiFe]-Hydrogenase complex from *Methanothermobacter marburgensis*, the first X-ray structure of a group 3 family member. *J. Mol. Biol*. **426**, 2813–2826 (2014).

61. Ousley, S., de Beer, D., Bejarano, S. & Chennu, A. High-resolution dynamics of hydrogen peroxide on the surface of scleractinian corals in relation to photosynthesis and feeding. *Front Mar. Sci*. **9**, 812–839 (2022).

62. Rebelein, J. G. Methane formation driven by light and heat prior to the origin of life and beyond. *Edmond*, https://doi.org/10.17617/3.6X6JXR. (2023).

Acknowledgements

Author contributions

J.G.R. and L.E. conceived the project. J.G.R. supervised and administered the project. J.G.R., F.K., J.M.K., T.D. and L.E. acquired funding. L.E. and J.G.R designed and analyzed the experiments. L.E. performed the experiments. J.M.K. was involved in H_2O_2 microsensor and LED experiments (Figs. 3B, 4B, Supplementary Fig. 3). U.B. measured H_2O_2 formation (Supplementary Figs. 2, 5 and 10). J.H. measured methanol formation (Supplementary Fig. 6). L.E. and J.G.R. conceptualized, visualized and wrote the original draft. J.G.R., LE, FK and JMK edited the draft. All authors read and reviewed the manuscript.

Funding

Competing interests

The authors declare no competing interests.

Additional information

Supplementary information The online version contains supplementary material available at https://doi.org/10.1038/s41467-023-39917-0.

Correspondence and requests for materials should be addressed to Leonard Ernst or Johannes G. Rebelein.

Peer review information Nature Communications thanks the anonymous reviewer(s) for their contribution to the peer review of this work. A peer review file is available.

Reprints and permissions information is available at http://www.nature.com/reprints

Publisher's note Springer Nature remains neutral with regard to jurisdictional claims in published maps and institutional affiliations.